

Availability of Subsurface Water-Ice Resources in the Northern Mid-Latitudes of Mars

G. A. Morgan^{1*}, N. E. Putzig¹, M. R. Perry¹, H. G. Sizemore¹, A. M. Bramson², E. I. Petersen², Z. M. Bain¹, D. M. H. Baker³, M. Mastrogiuseppe^{4,5}, R. H. Hoover⁶, I. B. Smith¹, A. Pathare¹, C. M. Dundas⁷, B. A. Campbell⁸

¹Planetary Science Institute, AZ, USA.

²Lunar and Planetary Lab, University of Arizona, AZ, USA.

³NASA Goddard Space Flight Center, MD, USA

⁴California Institute of Technology, CA, USA

⁵University of La Sapienza, Rome, Italy

⁶Southwest Research Institute, CO, USA

⁷U.S. Geological Survey Astrogeology Science Center, Flagstaff, AZ, USA

⁸Smithsonian Institution, DC, USA

* gmorgan@psi.edu

Abstract

Multiple nations and private entities are pushing to make landing humans on Mars a reality. The majority of proposed mission architectures envision “living off the land” by leveraging Martian water-ice deposits for fuel production and other purposes. Fortunately for mission designers, water ice exists on Mars in plentiful volumes. The challenge is isolating accessible ice deposits within regions that optimize other preferred landing-site conditions. Here, we present the first results of the Mars Subsurface Water Ice Mapping (SWIM) project, which has the aim of searching for buried ice resources across the mid-latitudes. Through the integration of orbital datasets in concert with new data-processing techniques, the SWIM project assesses the likelihood of ice by quantifying the consistency of multiple, independent data sources with the presence of ice. Concentrating our efforts across a significant portion of the northern Hemisphere, our composite ice consistency maps indicate that the broad plains of Arcadia and the extensive glacial networks across Deuteronilus Mensae match the greatest number of remote sensing criteria for accessible ice-rich, subsurface material situated equatorward of the contemporary ice-stability zone.

Introduction

Within the constraints imposed by current propulsion technology, mass represents the ultimate premium for space travel. Harvesting Martian water to refuel human spacecraft prior to the return trip to Earth results in a significant cost saving in terms of initial launch mass reduction, and this activity has been a common element of mission concepts since the late twentieth century [1-2]. The most substantial accumulations of ice on Mars are found in kilometers-thick polar ice caps. These ice deposits would provide an ample feedstock for rocket propellant, but their high latitudes are extremely challenging for landed missions (see Box 1). Presently, consensus is lacking as to the full extent and depth of accessible (meters-deep) ice nearer to the equator than the high-latitude zones of ice stability.

In this Perspective we aim to explore the extent to which existing remote-sensing datasets can be applied to the search for buried, non-polar ice resources. To date, most investigators have concentrated their efforts in either isolated regions [e.g. 3] or working primarily with single datasets [e.g. 4], including the recent assessment of ice distribution by [5] using Mars Climate Sounder (MCS) data, typically with shallow (< ~1 m) sensing depths. Taking an integrated data approach, the aim of the SWIM project is to leverage the full suite of ice-sensitive datasets and techniques to search for areas of Mars that present the most lines of evidence for ice. We use neutron, thermal, image, elevation, and radar data to develop a flexible

methodology for data assimilation that helps constrain the limitations of the current datasets and is open to community refinement. Of course, safely delivering humans to Mars and ensuring their survival requires many other considerations beyond in situ utilization of water resources, including landing-site safety and solar/thermal specifications (Box 1). Defining such site requirements is beyond the scope of the SWIM project and would be premature, given that all human Mars mission plans are still in the conceptual stage. However, due to the fundamental importance of water resources, we provide a hemispheric perspective of ice distribution to support initial landing-site studies and enable the community to explore the range of Martian terrains that host ice (Fig. 1).

Searching for ice on Mars

Subsurface ice that is accessible as a resource within the scope of technology currently in development (upper few meters) is predicted to have been deposited from atmospheric water vapor and to be stable presently from the poles down to the upper mid-latitudes [6-8]. Numerical modelling work, leveraging both measured surface conditions (elevation and thermal properties) and calibrated via neutron-spectrometer measurements [9], has provided detailed maps of the current, shallow (1–3 m deep) ice stability zone (Figure 1a) [8]. While understanding the location of ice that is in equilibrium with the atmosphere at present day is of value to mission planners, significant amounts of ice could exist out of equilibrium and the pore spaces of theoretically stable zones could be incompletely filled with ice.

Our evolving understanding of recent climate change has revealed the dynamic nature of Martian ice stability, including the occurrence of “ice ages” corresponding to near-global deposition of surface ice [10]. Research drawn from Mars missions has found evidence of extensive, relict ice-rich deposits in the middle and lower mid-latitudes of Mars. Glacial deposits, some >1 km thick, have been discovered through a combination of geomorphologic [e.g. 11-12] and radar sounding [e.g. 13-14] studies. Additionally, the recent identification of mid-latitude subsurface ice sheets [15], combined with ice-exposing impacts [16-17] and a prevalence of smaller-scale periglacial landforms [e.g. 18] within these latitudes, further hint at the widespread preservation of ice deposited during previous climate regimes. Maps of ice resources therefore need to include all available shallow ice deposits, irrespective of the age and emplacement mechanisms of the ice.

Box 1. From robots to humans: defining an acceptable landing site.

To date, nine missions have successfully landed and operated at least briefly on the surface of Mars. The choices of landing site for these missions represent compromises made between science goals and available technology. Regardless of the specifics, mission designers also have to contend with two main considerations: (1) ensuring the landing-zone properties are within the engineering thresholds of the descent and landing system and (2) identifying a landing-site environment conducive to surface operations. With regards to the former, attention needs to be given to surface roughness (on a range of scales from >100 m baselines down to <1 m boulder distributions [e.g. 38]) in addition to ensuring the density of the near surface is sufficient to provide accurate altimetry from the descent radar system [e.g. 39]. As every past Mars lander has used a parachute to reduce velocity during transit through the Martian atmosphere, the atmospheric pressure places a critical limit on landing sites: no successful mission has touched down on the surface above an altitude of -1380 m (except for the Soviet Mars 3 probe, which failed after an initial surface transmission). When contemplating surface operations, insolation is a critical factor, not only for missions reliant on solar power, but also to provide a manageable thermal environment. For example, despite the continuous electricity generated by Curiosity’s radioisotope power system, balancing the onboard heating budget (essential to support rover operations, from electronic functionality to actuator lubricant viscosity [40]) with that of the energy needs of the science payload dictated a landing site at latitudes below 30° [39].

Many of these landing-site considerations are also applicable to future human missions. As a consequence, ice resources at lower latitudes (higher annually averaged solar zenith angle, i.e., higher insolation and temperatures) and lower elevations (i.e., thicker atmosphere) will be considered of the

highest “value” to mission architects. The constant presence of orbital robotic missions at Mars since the 1990s has afforded us a detailed understanding of the surface environment. Thus, it is possible to accurately predict available solar-power resources for any spot on the planet [e.g. 42-42] as well as to explore the surface conditions required for landing safety at sub-meter resolutions [e.g. 43]. The vital missing piece of the puzzle for human-mission planners is the location and properties of available water-ice resources.

Mars Subsurface Water Ice Mapping (SWIM) project

In 2015, NASA hosted a Human Landing Site Selection (HLS2) Workshop to facilitate community-led landing-site suggestions. In addition to hosting targets of scientific significance, each landing-site proposal was required to identify a source of H₂O feedstock (ice and/or hydrated minerals). At this first HLS2 Workshop, 46 locations were put forward, spanning a broad range of terrain types. With the aim of further refining site selection, NASA commissioned pilot studies in 2017 that led to the Mars SWIM project in 2018 to provide the community with ice-resource map products. The Mars SWIM team set out to (1) produce maps of shallow ice distribution (upper 5 m) through data assimilation and, where possible, (2) quantify ice volume through thickness estimates of potential ice-rich deposits.

Our methodology leverages five independent remote sensing techniques, including neutron spectroscopy, thermal analysis, radar surface analysis, radar subsurface compositional (dielectric) analysis, and geomorphic mapping of periglacial features. In our analysis of each of these five datasets, we attempt to isolate distinct properties of the subsurface that provide proxies for the presence (or absence) of ice (see *Ice Characterization Techniques* subsection below). For example, we use the thermal datasets to look for regions with high subsurface thermal inertia, consistent with ice, whereas we apply the radar surface analysis to track evidence of ice-like low-density materials. The majority of these techniques also represent significant advancements on previous, similar methodologies. For instance, our thermal analysis provides a factor of 4 improvement in resolution and enhanced coverage relative to that of [19] and our radar subsurface dielectric analysis pioneered the use of regional networks of topographical controls to improve compositional estimates relative to that of [20].

To establish the feasibility of our approach, we concentrated our mapping efforts in the Martian northern plains from the equator to 60°N and from 290°E to 225°E (Fig. 1a). This lower latitude, lower elevation study region was chosen to broadly satisfy mission landing and operational considerations (Box 1) and because of previous detections of potentially extensive ground ice [e.g. 20]. The region also accounts for almost half (20) of the 46 locations presented at the HLS2 workshop.

Ice Characterization Techniques

Here we review the orbital datasets and methodology behind each technique. The specific conversion to individual ice consistency values is explained in the Supplementary Material.

Neutron detection (“N”): The energy spectrum of (top of the atmosphere) neutron flux is highly sensitive to the presence of hydrogen atoms within the upper meter of the surface [21] and thus can be used to search for buried H₂O. We used the global two-layer maps of water-equivalent hydrogen (WEH) calculated by [4], which were derived from Mars Odyssey Neutron Spectrometer (MONS) data using the crossover technique devised by [9]. Specifically, we incorporated the values of W_{dn} (the WEH of the lower layer), which is the parameter most relevant to the water-ice content of the subsurface [4].

Thermal analysis (“T”): Thermal inertia, as derived from surface temperature observations, is influenced by rock abundance and the size, distribution, and induration of surface and subsurface granular materials [22] and can be used to constrain such physical properties of the near surface [e.g. 23]. Employing data from the Mars Global Surveyor (MGS) Thermal Emission Spectrometer (TES) and the Mars Odyssey Thermal Emission Imaging System (THEMIS), our technique exploits seasonal variations in apparent thermal inertia (ATI) to glean information about the heterogeneity of the Martian surface [19; 23]. By comparing variations in ATI derived from observations to that from numerical thermal models of

heterogeneous surfaces, we can distinguish layers and horizontal mixtures of different materials—including the presence of subsurface ice or ice-cemented soil—at each pixel (see Supplementary Fig. 1).

Geomorphic Mapping (“G”): The morphology of the Martian landscape can be surveyed to search for evidence of subsurface ice. Using Mars Reconnaissance Orbiter (MRO) Context Camera (CTX) image mosaics [24], we applied a modified grid-mapping approach [25] to survey the presence of 10 periglacial landforms and terrain types proposed to contain ice (see Supplementary Information).

Radar surface analysis (“RS”): MRO Shallow Radar (SHARAD) echoes returned from the “surface” (upper 5 m) of Mars are a function of Fresnel reflectivity, which in turn provides a measure of near-surface density. Due to the low density of ice, measuring reflectivity offers a strategy to search for near-surface ice-rich deposits. To isolate Fresnel reflectivity from the multiple parameters contained in the power return [26] (including surface roughness) we followed a methodology first attempted with MARSIS sounder data [27] and later applied to SHARAD data [26; 28]. Taking a new direction, we normalized the power using the SHARAD roughness parameter [29] (see Supplementary Information).

Radar subsurface dielectric analysis (“RD”): Following on the technique developed in [13], we examined the complete SHARAD coverage of the study region to search for subsurface reflections produced by dielectric contrasts (see Supplementary Fig. 2). Taking advantage of all available topographic controls to estimate the depth of the reflectors we used the radar-measured time delay to constrain the relative dielectric permittivity (ϵ') of the subsurface, which in turn can inform the ice content (see Supplementary Information).

Assessing ice distribution through consistency mapping

Inferring the presence of shallow ice with high confidence from multiple, independent techniques is challenging, because the supporting datasets: (1) probe to different depths into the subsurface (see Supplementary Fig. 3), (2) have different footprints, (3) have varying coverage/quality, and (4) possess distinct caveats associated with distinguishing ice from other materials. Nevertheless, such an endeavor is not without precedent within the terrestrial literature. To reconcile contrasting views of the state of the (near-inaccessible) base of the Greenland ice sheet, [30] tracked areas of agreement between remote sensing datasets and models. Following the rationale that mutually confirming signatures of basal melt hold more significance than a single positive result enabled the production of a new, congruent map of the base of the entire ice sheet. Taking a similar approach, we have developed a means to quantify values of “ice consistency” (C), a parameter that tabulates the degree to which each technique supports or refutes the presence of near-surface ice. As each technique is based on actual instrument measurements, combining the collective results (see Supplementary Fig. 4) for a specific location provides a tangible representation of the cumulative evidence of accessible ice. To that end, we have developed the SWIM equation (Eq. 1) to calculate composite ice consistency, C :

$$C_i = (C_N + C_T + C_G + C_{RS} + C_{RD}) / 5 \quad (1)$$

Each subscript of the individual consistency terms refers to the relevant ice characterization technique outlined above. Rather than apply a binary result – ice/no ice - to each of the terms in Eq. 1, we instead convert the values measured by each remote sensing technique into consistency values that range from -1, meaning wholly inconsistent with ice, to +1, meaning wholly consistent with ice. A value of 0 means the data are inconclusive or missing. The conversion process is specific to each ice-detection technique and is outlined in the Supplementary Information (see Supplementary Table 1). We note that C_i should be interpreted as an indication of the consistency of the evidence for ice across multiple data sets and does not itself indicate anything about abundance or distribution of ice (within the collective probing depths of the techniques: >5m). The evidence from each data type should be assessed independently to facilitate such interpretations.

When interpreting C_i values, it is important to note the variable depth of information of each technique (see Supplementary Fig. 3), their relative sensitivity to the presence of ice, and the potential to produce false negatives and positives. For example, neutron data are very sensitive to the presence of water ice down to concentrations as low as 1%, but a relatively thin dry overburden on the order of 50 cm would prevent even a pure 100% ice deposit from being detected. Conversely, the radar surface return is a proxy for bulk density over the upper 5 m, and thus an ice-rich regolith can appear indistinguishable from meters-thick accumulations of low-density material such as dust. Considering the properties of each technique, a maximum C_i value of +1 requires that all techniques unequivocally support the presence of ice, and would translate to a nearly pure ice deposit that is >5 m in thickness and exhibits a recognized Martian ice-related morphology. While such a scenario would be highly advantageous to human missions, ice in lower concentrations and/or buried by a thin overburden also constitutes viable resources.

C_i values of at least +0.2 would be equivalent to one technique registering a high confidence in the presence of ice and the other four being agnostic. Any C_i value >0.2 therefore requires that more than one technique supports the presence of ice. Similarly, C_i values >0.5 require a majority of techniques (at least three of the five) to register high individual ice consistency values. Thus, we consider $C_i = 0.2$ a minimum threshold for initial mission planning and $C_i > 0.5$ to represent areas of the maximum interest. It should be noted that we treat negative and positive values equally, hence, in the case of map pixels that register both negative and positive inferences of ice, it will be the mean degree of confidence in these inferences that determine whether the final C_i value is positive or negative.

Our mapping shows that positive C_i pixels correlate, to an extent, with previous ice-stability modeling (Fig. 1). For most longitudes, significant C_i values (>0.2) form a band poleward of 50° that is contained within the zone of ice stability as predicted by [8]. In contrast, within the Arcadia Planitia – Phlegra Montes region, the high C_i band extends significantly beyond the modeled ice stability zone, and other, less pervasive patches of $C_i > 0.2$ exist farther south.

Comparison with fresh ice-exposing impact sites.

To evaluate our ice consistency methodology, we applied a form of ground-truth assessment by comparing our mapping results to the locations of fresh, ice-exposing impacts [16-17] (Fig. 2). Within our study region, 14 of the 15 ice-exposing impacts are located within pixels of positive C_i values, including the lowest latitude (39°N) impact site (average C_i value of 0.26 ± 0.16 ; see Supplementary Table 2). The one exception is in a pixel that has a low negative (essentially inconclusive) C_i value of -0.05 but is surrounded by positive C_i pixels. In good agreement with our mapping, all of the ice-exposing impacts located outside of the predicted ice-stability zone are clustered within the region of elevated C_i in Arcadia Planitia – Phlegra Montes (Fig. 2).

Measuring potential ice deposit thickness

Depending on the exact mission parameters and available technology, deeper, voluminous expanses of ice may be preferable to thin, shallow deposits. Producing volume estimates of ice resources was therefore a priority of the SWIM project and was achieved as part of the SHARAD subsurface mapping efforts, which form the basis of the *RD* analysis. To generate depth estimates of ice-rich deposits, we selected SHARAD subsurface reflectors that matched the following criteria: (i) they are located in regions of positive C_i and (ii) they express low dielectric permittivity values (and thus are compatible with the presence of ice). The corresponding dielectric permittivity estimates were used to constrain the thickness of units that exhibit an elevated ice content (relative to the surrounding terrain) by converting the time delay of the reflectors to depth (Fig. 3–4).

Most promising regions

High C_i values (>0.5) are found both as a broad concentration within the Arcadia southern excursion as well as within more discretely distributed patches across the study area (Fig. 1, 2, and 4). Regarding the

latter, high C_i values are associated with the ejecta blankets of impact craters in eastern Utopia Planitia, including the 100 km diameter Mie crater, though the most southern ($\sim 35^\circ$ N) elevated C_i values are correlated with glacial features within Deuteronilus Mensae [e.g. 12] (Fig. 3). Previous radar studies of Deuteronilus [14, 31] measured high bulk ice content within the glacial deposits. Our mapping expanded upon these studies and returned further support for the presence of massive ice (average ϵ' of 3.4 ± 0.5). We also built upon radar studies of mantling units located in the plains adjacent to the glaciers by [32] (Fig. 3). Our ϵ' estimate for the mantles of 4.0 ± 1.0 is higher than that of the glaciers (though less well constrained), but is still consistent with the presence of ice. Interestingly, the newly developed RS technique, displays contrasting results from the mantle and the glacial units (Fig. 3). Low-power returns suggestive of low-density material is measured over the glaciers. Because the RS is sampling only the upper ~ 5 m, this suggests that either the glacial ice is buried by a very thin (< 2 m) debris cover or alternatively the overburden is composed of meters-thick, highly porous material. In contrast, the mantling units exhibit higher-power RS returns, which argue against the presence of ice (Fig. 3), possibly indicating that any ice still preserved in these deposits is buried at greater depth, below a desiccated surficial layer.

In the case of Arcadia, the high C_i values extend across young volcanic terrains including possible > 1800 km long, pre-aureole Olympus Mons lava flows [33]. The high C_i values also spatially correlate with the widely distributed subsurface reflector described by [20], which was interpreted to consist of a mantling unit comprising massive ice (dielectric constant, ϵ' , of 2.5 ± 0.3). Through our new RD mapping, the reflector was found to be more spatially extensive, extending down to 36° N and expressing depths of 15 to > 100 m (Fig. 4). Building upon [20], we applied a more widely distributed network of topographic controls to estimate the permittivity of the material bounded by the reflector. Our revised ϵ' estimate for the mantling material is 4.6 ± 1.2 . While higher than the dielectric constant of the Deuteronilus Mensa glacial deposits (~ 3), the mean Arcadia value is significantly lower than that of lava flows studied in other Amazonian volcanic regions [34-35]. This suggests a moderately compacted sedimentary unit as opposed to a weathered lava flow complex. The loss tangent values in several thicker locations are likewise about a factor of 3 higher than those of the Deuteronilus deposits [36], so any ice must be at a low overall fraction rather than extending from the surface to the depth of the reflector. The sounder data do not preclude a modest component of ice, and as the independent N, T, and G techniques have high confidence levels in this region, we infer that ice is present close to the surface in Arcadia.

Perspectives and future applications

Our multi-technique ice-consistency map advocates for the availability of ice resources equatorward of the modeled zone of ice stability [e.g. 8]. The diverse nature of the most promising mid-latitude regions suggests a range of potential landing site environments will be available for future selection. Undertaking an integrated approach has provided new insights into the nature and spatial distribution of ice, even in regions that had previously been the focus of investigations such as Deuteronilus and Arcadia. Leveraging the different probing depths of the individual techniques has also enabled us to constrain the concentration of ice within the vertical column, further demonstrating the benefits of multi-dataset assimilation. From a science perspective, the likely presence of such diverse, ice-rich deposits equatorward of the current ice stability zone also provide a means with which to track climatic fluctuations through Martian history.

This Perspective also serves as a broad assessment of the utility of existing datasets in searching for ice within the upper few meters of the Martian subsurface. A significant knowledge gap exists for depths between 0.5 m and 15 m. While SHARAD surface analysis offers valuable insight into the upper ~ 5 m, the returned measurements provide bulk estimates, preventing a finer-scale delineation of the dry overburden that shields ice deposits out of equilibrium with the current climate. New instrumentation, including (but not limited to) higher-frequency synthetic-aperture imaging and sounding radars, would provide a critical advance toward assessing shallow ice content for both resource and science applications [37].

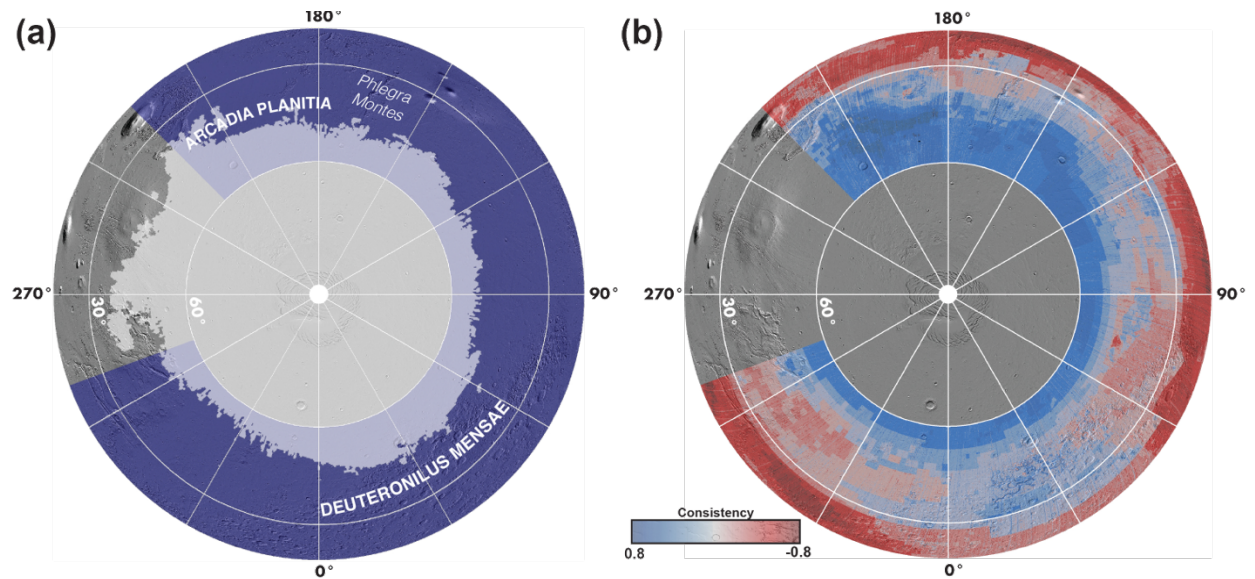


Fig. 1 | Mars SWIM Project study region and ice consistency results. (a) Study region (purple shading) and estimated areal extent of northern hemisphere theoretical 3-m ice stability (grey shading) under current atmospheric conditions [8]. (b) Map of composite ice consistency, C . Positive (blue) pixels are consistent with presence of ice, negative (red) pixels are consistent with the absence of ice. All map products are overlain on Mars Orbiter Laser Altimeter (MOLA) shaded relief (grey background) in a north polar orthographic projection.

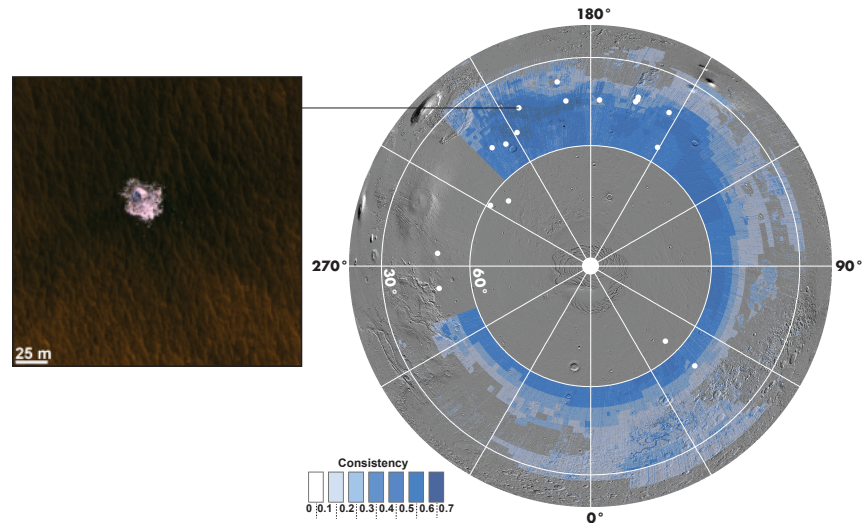


Fig. 2 | Correlation between ice-exposing, fresh impacts and positive C_i values. Map of positive C_i (consistent with the presence of ice) across the study area overlain by the location of ice-exposing fresh impacts (white dots). The insert contains an example of an ice-exposing impact within Arcadia (HiRISE image ESP_025840_2240).

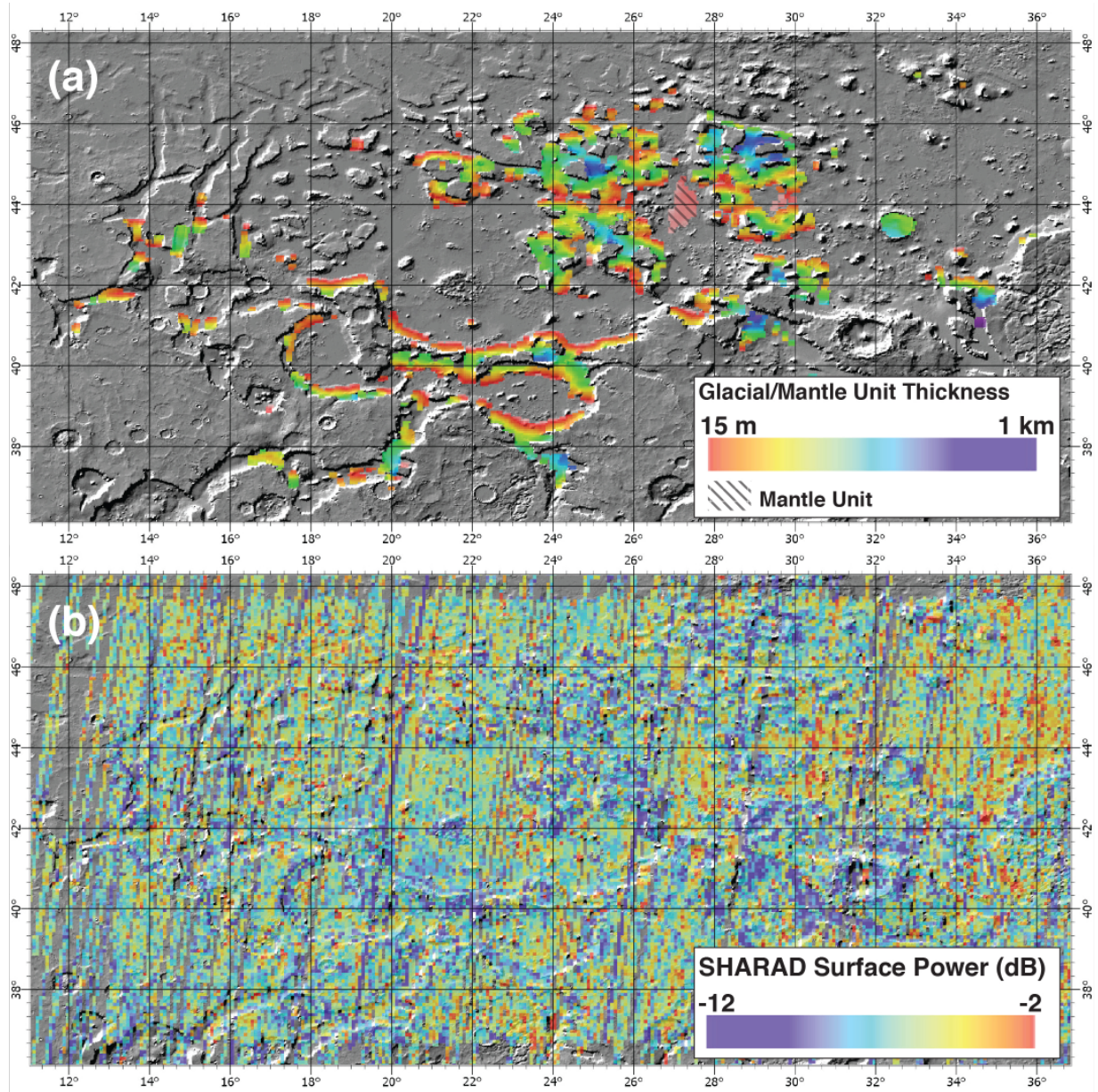


Fig. 3 | Radar analysis (RS/RD) of glaciers and mantle deposits within Deuteronilus Mensae (a) Depth to base of glacial deposits and mantle units and (b) corresponding radar surface analysis of the region. Note, low-power returns (consistent with the presence of ice in the upper 5 m) correlate with the surfaces of the glaciers.

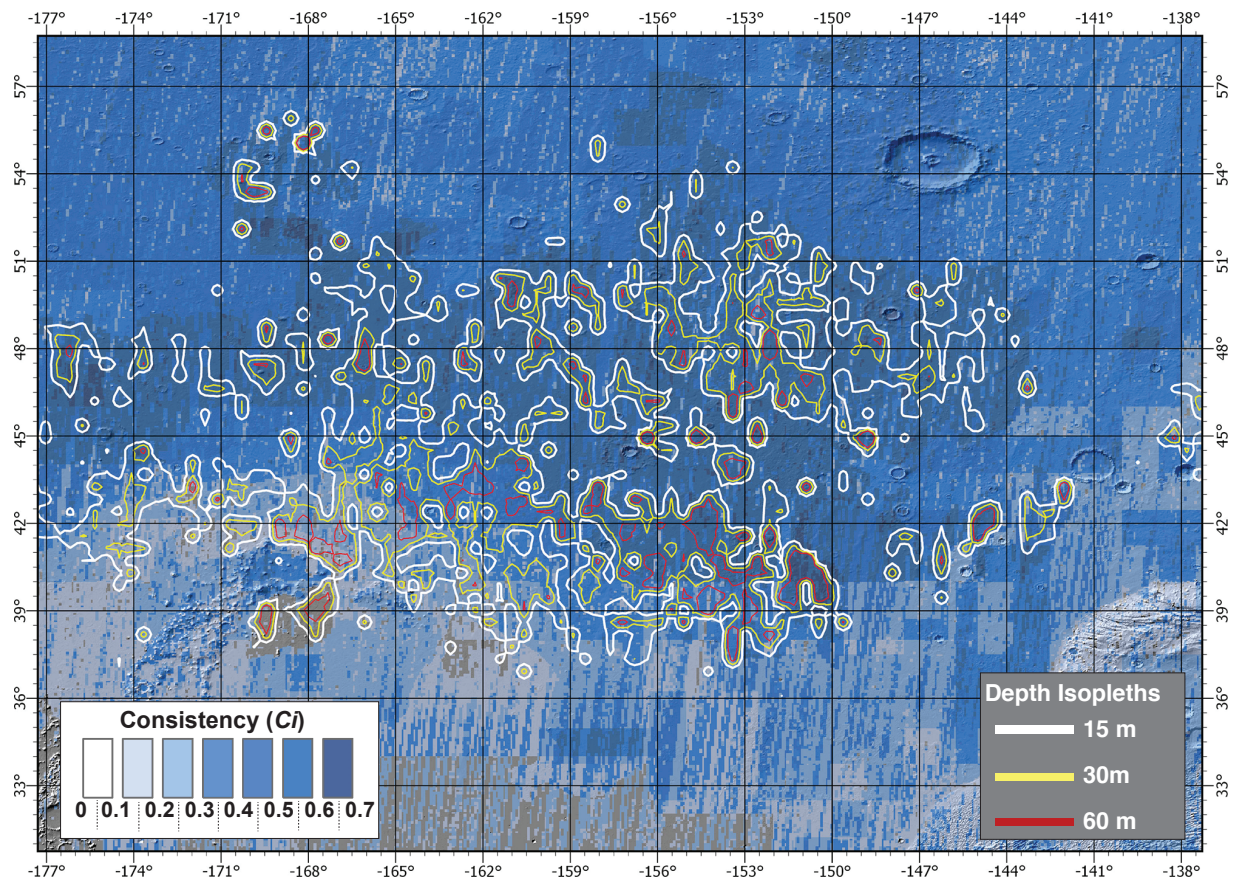


Fig. 4 | Spatial extent and thickness of deposits identified within the high C_i (ice-rich) Arcadia region. Comparing the individual response of the different techniques suggests that ice is concentrated in the near surface. C_i map overlaid with deposit isopachs determined from mapped subsurface radar reflectors.

Data availability

The ice consistency and thickness maps (as both GIS-compatible GeoTIFFs and browse images) along with the constituent data for each ice-detection technique are available on the Subsurface Water Ice Mapping (SWIM) Project website at: <https://swim.psi.edu>. All of the instrument datasets used to derive our ice detection techniques are available on the NASA Planetary Data System: <https://pds.nasa.gov/>. The Dickson et al [24] CTX mosaic used to tabulate the geomorphology ice consistency values can be found on the Caltech Murray Lab website at: <http://murray-lab.caltech.edu/CTX/index.html>. Updates of new SWIM products can be found at <https://twitter.com/RedPlanetSWIM>.

References

1. Zubrin, R., Daker, D., and Gwynne, O. Mars Direct: A simple, robust, and cost effective Architecture for the Space Exploration Initiative, 29th Aerospace Sciences Meeting, No. AIAA-91-329 (1991)

2. Ash, R. L., Dowler, W. L., and Varsi, G., Feasibility of rocket propellant production on Mars, *Acta Astronautica*, Vol. 5,, pp. 705–724 (1978)
3. Baker, D.M.H., Head, J.W. Extensive Middle Amazonian mantling of debris aprons and plains in Deuteronilus Mensae, Mars: implications for the record of mid-latitude glaciation. *Icarus* 260, 269–288. <https://doi.org/10.1016/j.icarus.2015.06.036> (2015)
4. Pathare, A.V., Feldman, W.C., Prettyman, T.H., and Maurice, S. Driven by excess? Climatic implications of new global mapping of near-surface water-equivalent hydrogen on Mars. *Icarus* 301, 97–116, doi:10.1016/j.icarus.2017.09.031 (2018)
5. Piqueux, S., Buz, J., Edwards, C. S., Bandfield, J. L., Kleinböhl, A., Kass, D. M., et al. Widespread shallow water ice on mars at high latitudes and midlatitudes. *Geophys. Res. Lett.*, 46, 14290– 14298. <https://doi.org/10.1029/2019GL083947> (2019)
6. Leighton, R. B., & Murray, B. C. Behavior of carbon dioxide and other volatiles on Mars. *Science*, 153(3732), 136 LP – 144. <https://doi.org/10.1126/science.153.3732.136> (1966)
7. Paige, D. A. The thermal stability of near-surface ground ice on Mars, *Nature*, 356, 43–45, doi:10.1038/356043a0 (1992)
8. Mellon, M. T., W. C. Feldman, and Prettyman, T. H. The presence and stability of ground ice in the southern hemisphere of Mars, *Icarus*, 169, 324–340, doi:10.1016/j.icarus.2003.10.022 (2004)
9. Feldman, W.C., Pathare, A., Maurice, S., Prettyman, T.H., Lawrence, D.J., Milliken, R.E. and Travis, B.J. Mars Odyssey neutron data: 2. Search for buried excess water ice deposits at nonpolar latitudes on Mars. *J. Geophys. Res.*, 116(E11) (2011)
10. Head, J. W., Mustard, J. F., Kreslavsky, M. A., Milliken, R. E., & Marchant, D. R. Recent ice ages on Mars. *Nature*, 426(6968), 797–802. <https://doi.org/10.1038/nature02114> (2003)
11. Squyres, S. W. The distribution of lobate debris aprons and similar flows on Mars, *J. Geophys. Res.*, 84 (B14), 8087– 8096, doi:10.1029/JB084iB14p08087 (1979)
12. Head, J. W. et al. Extensive valley glacier deposits in the northern mid-latitudes of Mars: Evidence for Late Amazonian obliquity-driven climate change. *Earth and Planetary Science Letters*. 241 (3): 663–671. (2006)
13. Holt, J. W., Safaeinili, A., Plaut, J. J., Head, J. W., Phillips, R. J., Seu, R., Kempf, S. D., Choudhary, P., Young, D. A., Putzig, N. E., Biccari, D., Gim, Y. Radar sounding evidence for buried glaciers in the southern mid-latitudes of Mars. *Science* 322, 1235–1238, doi:10.1126/science.1164246 (2008)
14. Plaut, J. J., A. Safaeinili, J. W. Holt, R. J. Phillips, J. W. Head, R. Seu, N. E. Putzig, and Frigeri, A. Radar evidence for ice in lobate debris aprons in the mid-northern latitudes of Mars, *Geophys. Res. Lett.*, 36(L02203), 1–4, doi:10.1029/2008GL036379 (2009)
15. Dundas, C. M., Bramson, A. M., Ojha, L., Wray, J. J., Mellon, M. T., Byrne, S., McEwen, A. S., Putzig, N. E., Viola, D., Sutton, S., Clark, E., Holt, J. W. Exposed subsurface ice sheets in the Martian mid-latitudes. *Science*, 359(6372), 199 LP – 201 (2018)
16. Byrne, S., Dundas, C.M., Kennedy, M.R., Mellon, M.T., McEwen, A.S., Cull, S.C., Daubar, I.J., Shean, D.E., Seelos, K.D., and Murchie, S.L. Distribution of mid-latitude ground ice on Mars from new impact craters. *Science* 325, 1674–1676 (2009)
17. Dundas, C.M., Byrne, S., McEwen, A.S., Mellon, M.T., Kennedy, M.R., Daubar, I.J., and Saper, L. HiRISE observations of new impact craters exposing Martian ground ice. *J. Geophys. Res.* 119, 109–127, doi:10.1002/2013JE004482 (2014)
18. Milliken, R.E., Mustard, J.F., Goldsby, D.L. Viscous flow features on the surface of Mars: Observations from high-resolution Mars Orbiter Camera (MOC) images. *J. Geophys. Res.*, Planets 108 (E6). doi:10.1029/2002je002005 (2003)
19. Putzig, N. E., & Mellon, M. T. Apparent thermal inertia and the surface heterogeneity of Mars. *Icarus*, 191(1), 68–94. <https://doi.org/10.1016/j.icarus.2007.05.013> (2007)

20. Bramson, A.M., Byrne, S., Putzig, N.E., Sutton, S., Plaut, J.J., Brothers, T.C., and Holt, J.W. Widespread excess ice in Arcadia Planitia, Mars. *Geophys. Res. Lett.* 42, 6566– 6574, doi:10.1002/2015GL064844 (2015)
21. Feldman, W.C., Prettyman, T.H., Maurice, S., Plaut, J.J., Bish, D.L., Vaniman, D.T., Mellon, M.T., Metzger, A.E., Squyres, S.W., and Karunatillake, S. Global distribution of near-surface hydrogen on Mars. *J. Geophys. Res.* 109, E09006, doi:10.1029/2003JE002160 (2004)
22. Mellon, M. T., Fergason, R. L., and Putzig, N. E. The thermal inertia of the surface of Mars. in *The Martian Surface: Composition, Mineralogy, and Physical Properties* (ed. Bell III, J. F.) 399–427, Cambridge Univ. Press (2008)
23. Putzig, N. E., Mellon, M. T., Herkenhoff, K. E., Phillips, R. J., Davis, B. J., Ewer, K. J., & Bowers, L. M. Thermal behavior and ice-table depth within the north polar erg of Mars. *Icarus*, 230, 64–76. <https://doi.org/10.1016/J.ICARUS.2013.07.010> (2014)
24. Dickson, J. L., Kerber, L. A., Fassett, C. I., Ehlmann, B. L. A global, blended CTX mosaic of Mars with vectorized seam mapping: A new mosaicking pipeline using principles of non-destructive image editing. LPSC #2480 (2018)
25. Ramsdale, J. D., Balme, M. R., Gallagher, C., Conway, S. J., Smith, I. B., Hauber, E., et al. Grid mapping the northern plains of Mars: Geomorphological, radar, and water-equivalent hydrogen results from Arcadia Planitia. *J. Geophys. Res.*, 124, 504– 527. <https://doi.org/10.1029/2018JE005663> (2019)
26. Grima, C., W.Kofman, A. Hérique, R. Orosei, and Seu, R. Quantitative analysis of Mars surface radar reflectivity at 20MHz, *Icarus*, 220,84–99, doi:10.1016/j.icarus.2012.04.017 (2012)
27. Mouginot, J., et al. The 3–5 MHz global reflectivity map of Mars by MARSIS/Mars Express: Implications for the current inventory of subsurface H₂O, *Icarus*, 210, 612–625, doi:10.1016/j.icarus.2010.07.003 (2010)
28. Castaldo, L., Mège, D., Gurgurewicz, J., Orosei, R., & Alberti, G. Global permittivity mapping of the Martian surface from SHARAD. *Earth Planet. Sci. Lett.*, 462, 55–65. <https://doi.org/https://doi.org/10.1016/j.epsl.2017.01.012> (2017)
29. Campbell, B. A., N. E. Putzig, L. M. Carter, G. A. Morgan, R. J. Phillips, and J. J. Plaut, Roughness and near-surface density of Mars from SHARAD radar echoes, *J. Geophys. Res.*, 118, 436–450, doi:10.1002/jgre.20050 (2013).
30. MacGregor, J. A., et al. A synthesis of the basal thermal state of the Greenland Ice Sheet, *J. Geophys. Res. Earth Surf.*, 121, 1328– 1350, doi:10.1002/2015JF003803 (2016)
31. Petersen, E. I., J. W. Holt, and Levy, J. S. High ice purity of Martian lobate debris aprons at the regional scale: Evidence from an orbital radar sounding survey in Deuteronilus and Protonilus Mensae, *Geophys. Res. Lett.*, 45(21), 11,595–11,604, doi:10.1029/2018GL079759 (2018)
32. Baker, D.M.H., Carter, L.M. Radar reflectors associated with an ice-rich mantle unit in Deuteronilus Mensae, Mars. 48th Lunar Planet. Sci. Conference Abstract number 1575 (2017)
33. Fuller, E.R., and Head, J.W. Olympus Mons, Mars: Detection of extensive preareole volcanism and implications for initial mantle plume behavior. *Geology*, 31. 175-178 (2003)
34. Carter, L. M., B. A. Campbell, J. W. Holt, R. J. Phillips, N. E. Putzig, S. Mattei, R. Seu, C. H. Okubo, and A. F. Egan, A. F. Dielectric properties of lava flows west of Ascraeus Mons, Mars, *Geophys. Res. Lett.*, 36, L23204, doi:10.1029/2009GL041234 (2009).
35. Simon, M. N., Carter, L. M., Campbell, B. A., Phillips, R. J., and Mattei, S. Studies of lava flows in the Tharsis region of Mars using SHARAD, *J. Geophys. Res.*, 119, 2291– 2299. doi:10.1002/2014JE004666 (2014)
36. Campbell, B. A., and Morgan, G. A. Fine-scale layering of Mars polar deposits and signatures of Ice Content in Nonpolar Material From Multiband SHARAD Data Processing, *Geophys. Res. Lett.*, 45(4), 1759–1766.;10.1002/2017GL075844 (2018)

37. MEPAG ICE-SAG, Final Report from the Ice and Climate Evolution Science Analysis group (ICE-SAG), Chaired by S. Diniega and N. E. Putzig, 157 pages, posted 08 July 2019 by the Mars Exploration Program Analysis Group (MEPAG) at <http://mepag.nasa.gov/reports.cfm> (2019)
38. Arvidson, R., et al. Mars Exploration Program 2007 Phoenix landing site selection and characteristics, *J. Geophys. Res.*, 113, E00A03, doi:10.1029/2007JE003021 (2008)
39. Golombek, M., Grant, J., Kipp, D. et al. Selection of the Mars Science Laboratory landing site space *Sci Rev* 170: 641. <https://doi.org/10.1007/s11214-012-9916-y> (2012)
40. Novak, K.S., Liu, Y., Lee, C.-J., Hendricks, S. Mars Science Laboratory Rover actuator thermal design, in 40th ICES Conference, Barcelona, Spain (2010)
41. Appelbaum, J., & Flood, D. J. Solar radiation on Mars. *Solar Energy*, 45(6), 353–363. [https://doi.org/10.1016/0038-092X\(90\)90156-7](https://doi.org/10.1016/0038-092X(90)90156-7) (1990)
42. Badescu, V. Available solar energy and weather forecasting on Mars surface. In: Badescu V. (eds) *Mars*. Springer, Berlin, Heidelberg (2009).
43. Golombek, M. Kipp, D. Warner, N. Daubar, I.J. Fergason, R. Kirk, R.L. Beyer, R. Huertas, A. Piqueux, S. Putzig, N. Campbell, B.A. Morgan, G. Charalambous, C. Pike, W. Gwinner, K. Calef, F. Kass, D. Mischna, M. Ashley, J. Banerdt, W. Selection of the InSight landing site. *Space Sci. Reviews.*, 1-91. 10.1007/s11214-016-0321-9 (2016)

All correspondence and requests for materials should be addressed to G.A. Morgan.

Acknowledgments

The Subsurface Water Ice Mapping (SWIM) in the Northern Hemisphere of Mars project outlined in this paper was supported by grants provided by NASA through the Jet Propulsion Laboratory (JPL Subcontract No. 1611855; JPL RSA: 1589197 and 1595721). Elements of the ice detection techniques were pioneered through support provided to team members by the NASA Mars Reconnaissance Orbiter Project. PSI also acknowledges SeisWare International Inc. for an academic license of their software that was used for the SHARAD subsurface mapping. Any use of trade, firm, or product names is for descriptive purposes only and does not imply endorsement by the U.S. Government.

Author contributions

GAM and NEP led the project and wrote the majority of the manuscript. NEP, HGS, RHH, ZMB, and MRP conducted the *T* analysis. AMB, EIP, ZMB, MM, and MRP undertook the *RD* mapping and analysis. DMHB led the *G* mapping. GAM and BAC derived the *RS* products. MRP set up the computational and website infrastructure and archiving. MRP, ZMB, and GAM were responsible for producing the integrated *C* products. AP, CMD, IBS, and BAC contributed to the broad analysis and assisted the other team members in the preparation of the manuscript.

Competing interests

The authors declare no competing interests.

Additional Information

None noted at this stage